

Capillary threads and viscous droplets in square microchannels

Thomas Cubaud^{1,a)} and Thomas G. Mason^{2,b)}

¹*Department of Mechanical Engineering, Stony Brook University, Stony Brook, New York 11794, USA*

²*Department of Chemistry and Biochemistry, Department of Physics and Astronomy, and California NanoSystems Institute, University of California-Los Angeles, Los Angeles, California 90095, USA*

(Received 16 November 2007; accepted 28 March 2008; published online 1 May 2008)

We experimentally study the formation and evolution of threads containing more viscous liquids surrounded by less viscous, immiscible liquids through hydrodynamic focusing in square microchannels. Over a large range of viscosities and interfacial tensions, five characteristic regimes of flow behavior are identified: threading, jetting, dripping, tubing, and displacement. We locate the boundaries between these regimes on a flow map based on the capillary number of each fluid. In the jetting and the dripping regimes, the droplet size is measured and related to fluid properties, flow parameters, and geometry. The critical thread length before jetting droplets and the critical length of a viscous tail before breakup in dripping are also examined. This study classifies and defines regimes of thread instabilities that can be used to produce supra- and subchannel size viscous droplets in an elementary microfluidic geometry. © 2008 American Institute of Physics.

[DOI: 10.1063/1.2911716]

I. INTRODUCTION

A wide variety of instabilities can arise when streams of miscible and immiscible liquids interact.^{1,2} Depending on the thermodynamic properties of the liquids, the driving stresses, and the flow geometries, a host of dynamic instabilities can result from many different physical mechanisms. A large number of these instabilities have been classified and identified. For instance, a fingering (i.e., “Saffman–Taylor”) instability can occur when a less viscous liquid is injected into a region containing a more viscous liquid at rest. Another common instability is the capillary (i.e., “Rayleigh”) instability that arises when a cylindrical thread or jet of one liquid is formed in an immiscible fluid. Surface tension drives an interfacial instability that creates varicose undulations of the thread, ultimately overcoming viscosity or inertia to cause the thread to break up into droplets. The capillary instability of jets, threads, and isolated droplets has been extensively studied and is the basis for creating emulsions, dispersions of droplets of one liquid in a different immiscible liquid.^{3–6} Amphiphilic surfactant molecules are usually present at small amounts in most emulsion formulations to inhibit the coalescence of newly formed droplets after the capillary instability has occurred. Surface flows of surfactant can induce variations in surface tension (i.e., the “Marangoni effect”), which can substantially alter the interfacial morphology and sizes of the resulting droplets.⁴ For instance, when surfactant molecules are concentrated at the end of a droplet, “tip streaming” can occur.^{7,8} In addition to these classic instabilities, other instabilities, including the folding⁹ and swirling¹⁰ instabilities of viscous threads flowing in a less viscous miscible liquid, can be induced in microfluidic channels.

The development of micro- and nanotechnologies has

facilitated the precise manufacturing of microfluidic devices.^{11–13} When combined with high-speed imaging, microfluidics offers a wealth of opportunities for fluid experimentalists as well as the possibility of exploring flow regimes that were previously difficult to access. In particular, direct observations of multiphase flows in porouslike media have received considerable attention during the past decade.^{14–22} Recently, microfluidic investigations have revealed the possibility of forming transitory dispersions of viscous miscible liquids by using continuous flows.¹⁰ Among the practical advantages of microfluidics are the precise control of geometries, the possibility of readily investigating the influence of fluids physicochemical properties on the flow, the ability of exploring short flow time scales and high strain rates, and the strong attenuation of the stresses due volume forces such as inertia and gravity. A result of microscale miniaturization, surface-to-volume ratios are large, and flows naturally emphasize phenomena associated with viscosity, interfacial tension, and wetting.

Droplet formation has been widely studied in various microgeometries, such as microchannel arrays,^{23–25} T-sections,^{26–29} hydrodynamic focusing,³⁰ membrane emulsification,³¹ flow focusing,^{32–35} and concentric injection.^{36,37} Droplet production in microsystems using continuous flows generally provides the advantage of generating a high degree of monodispersity among droplets. This property is particularly appealing since most industrial methods generally provide only emulsions that have a substantial polydispersity in the sizes of the droplets. Often, this is due to a lack of uniformity in the flow fields used to rupture droplets in typical emulsification vessels and mixing systems.³⁸ Although classic emulsions are generally comprised of microscale droplets, recent advances in applying extreme flows have provided methods for mass-producing “nanoemulsions” comprised of sub-100 nm droplets through capillary instabilities.^{39–41}

^{a)}Author to whom correspondence should be addressed. Electronic mail: thomas.cubaud@stonybrook.edu.

^{b)}Electronic mail: mason@chem.ucla.edu.

Most studies of droplet generation in microfluidic devices involve rather complex geometries that are characterized by at least two length scales in the mixing section. Variation between different specific devices generally makes it difficult to compare the results obtained by using them. Below the macroscopic scale, the effect of viscosity on multiphase flow has been studied for a relatively small viscosity ratio;⁴² it is usually neglected for larger systems, mainly due to the difficulty in creating reproducible conditions over the time scales that can be reasonably accessed in a laboratory-scale experiment. However, the interplay between viscosity effects and geometry is crucial in the context of probing the rheology of multiphase flows, non-Newtonian liquids, and complex fluids in microfluidic systems.^{43–46} Due to the complexities of the phenomena, one must pay special attention to the geometries and their associated flow regimes that also strongly depend on fluid properties and flow parameters. Ultimately, understanding and controlling phenomena associated with large viscosity contrasts, and even nonlinear viscoelasticity, will make it possible to precisely manipulate soft materials comprised of reactive solvents and solutes in microgeometries.

Here, we study the interplay between viscosity and interfacial tension effects on the formation of Newtonian threads and droplets by hydrodynamic focusing⁴⁷ into square microchannels, covering a large range of viscosity contrasts that is unprecedented. The geometry we use is highly symmetric and characterized by channels having identical square cross sections with a single edge length. Over a broad range of fluid properties and flow parameters, five distinct flow regimes, including threading, jetting, dripping, tubing, and displacement, are located on a flow map based on two capillary numbers, one associated with the more viscous liquid and the other associated with the less viscous liquid. The identification of the critical capillary number at which interfacial and viscous effects balance as well as the study of “stable” threads, corresponding to the two-fluid primary flows, provide us with a strong rationale for investigating jetting and dripping instabilities. In particular, we derive scaling laws related to supra- and subchannel droplet formation. Moreover, we measure the critical thread length before droplets are formed through jetting, and we determine the critical length of a viscous tail before breakup in dripping. Besides establishing quantitative relationships that will be useful in many practical microfluidic applications, this study provides a detailed understanding of the influence of interfacial tension effects on viscous fluid microtransport, and it clarifies the role of the outer and the inner viscosity on thread and droplet formation in microfluidic flows.

II. EXPERIMENTAL PROCEDURE

A. Microfluidic system

We use a compact hydrodynamic focusing geometry,⁴⁷ which consists of four microchannels with square cross sections of identical width h that intersect at right angles, forming a “cross channel.” Into the inlet channel, liquid 1 ($L1$) having viscosity η_1 is introduced at the volumetric flow rate Q_1 far away from the intersection. At the inlet of each side

channel, liquid 2 ($L2$) having viscosity η_2 is symmetrically introduced at a rate $Q_2/2$. As a result, $L2$ hydrodynamically focuses $L1$ in the center of the outlet channel. By contrast to other microfluidic geometries, the symmetric hydrodynamic focusing geometry presents the advantage of having a cross section that can be characterized by only one length scale h that is readily accessible over a wide range ($0.5 \leq h \leq 500 \mu\text{m}$) by using silicon-based microfabrication techniques.

We fabricate hard microfluidic modules out of glass and silicon. A double-side polished silicon wafer ($h=100 \mu\text{m}$ thick) is patterned by using microlithographic techniques, and microchannel designs are etched through with a deep reactive ion etching process. Each side of a microchannel is then anodically bonded to a slide of borosilicate glass, producing a glass/silicon/glass sandwich structure that provides optical access suitable for imaging microflows.¹⁸ This bonding process provides very robust sealing, especially for solvents with low surface tension. In addition, these hard microchannels offer excellent chemical resistance, do not deform or separate under high-pressure flows, and are not porous. We create a cross channel consisting of a perpendicular intersection of four straight channels. Liquids are injected at constant flow rates by using syringe pumps. A fiber light is placed on one side of the module to provide sufficient illumination for high-speed imaging by using a camera equipped with a high-magnification stage and lens, located on the opposite side. Since the top and bottom walls are made of borosilicate glass and the two sidewalls are made of silicon, all wall materials have nearly the same wetting properties with the fluids used in this study.

B. Fluids

We use the following fluids: silicone oils [polydimethylsiloxane (PDMS)], glycerol, isopropanol, ethanol, and aqueous and ethylic mixtures of glycerol. Glycerol mixtures are prepared to assess the influence of intermediate η_1 , η_2 and γ_{12} on two-fluid microflows. The viscosity ranges in cP are $50 \leq \eta_1 \leq 1214$ and $0.82 \leq \eta_2 \leq 50$. The interfacial tension range is $1.5 \leq \gamma_{12} \leq 30.4 \text{ mN m}^{-1}$. All liquids are Newtonian and their viscosities have been measured by using tube viscometers. Interfacial tensions are determined by using the du-Nouy ring⁴⁸ and the combined capillary rise methods.⁴⁹ Based on the values of γ_{12} , we define three groups of fluid pairs: $G1$ for low $\gamma_{12} \approx 2 \text{ mN m}^{-1}$ with PDMS oil in a continuous phase of ethanol or isopropanol (“oil-in-water” type); $G2$ for intermediate $\gamma_{12} \approx 8 \text{ mN m}^{-1}$ with ethanol-glycerol mixture in a continuous phase of PDMS (“water-in-oil” type); and $G3$ for large $\gamma_{12} \approx 30 \text{ mN m}^{-1}$ with various water-glycerol mixtures in a continuous phase of PDMS (“water-in-oil” type). Material properties of these pairs are shown in Table I.

For low γ_{12} ($G1$), droplets and threads of $L1$ can wet the microchannels walls for small capillary numbers Ca (see also Sec. VII C). For intermediate to large γ_{12} ($G2$ and $G3$), $L2$ is composed of PDMS oil, which strongly wets the microchannel walls, thereby inhibiting $L1$ from significantly wetting the walls. Besides wetting, no difference between oil-in-

TABLE I. Physicochemical properties of pairs of liquids ($L1$ and $L2$): η_1 and η_2 are corresponding viscosities, $\chi = \eta_1 / \eta_2$ is the viscosity ratio, and γ_{12} is the interfacial tension. For $L1$ marked by (*), the volume percentage of glycerol in the mixture is given. All properties are measured at room temperature.

| Pair | $L1$ | η_1 (cP) | $L2$ | η_2 (cP) | χ | γ_{12} (mN m ⁻¹) | Symbol |
|-------|----------------------|---------------|-------------|---------------|--------|-------------------------------------|--------|
| $G1A$ | PDMS oil | 500 | Isopropanol | 2.23 | 224 | 2.2 | ● |
| $G1B$ | ... | 100 | ... | 2.23 | 45 | 2.2 | ■ |
| $G1C$ | ... | 50 | ... | 2.23 | 22 | 2.0 | ◆ |
| $G1D$ | ... | 500 | Ethanol | 1.16 | 431 | 1.7 | ▲ |
| $G1E$ | ... | 50 | ... | 1.16 | 43 | 1.5 | ▶ |
| $G2A$ | Ethanol-glycerol 70* | 110 | PDMS Oil | 0.82 | 134 | 7.2 | ⊗ |
| $G2B$ | ... | 110 | ... | 4.59 | 24 | 8.4 | ⊠ |
| $G3A$ | Glycerol | 1214 | PDMS Oil | 0.82 | 1484 | 26.6 | ○ |
| $G3B$ | ... | 1214 | ... | 4.59 | 264 | 27.0 | □ |
| $G3C$ | ... | 1214 | ... | 50 | 24 | 27.0 | ◇ |
| $G3D$ | Water-glycerol 92* | 360 | ... | 0.82 | 440 | 28.2 | ▷ |
| $G3E$ | Water-glycerol 80* | 77 | ... | 0.82 | 94 | 30.4 | △ |

water and water-in-oil types of emulsification are observed since no surfactants are used in this study. By varying the fluid pairs and the flow rates ($0.1 < Q_i < 200 \mu\text{l}/\text{min}$) at fixed h , we gather a comprehensive set of observations covering capillary numbers $Ca_i = \eta_i J_i / \gamma_{12}$, where $J_i = Q_i / h^2$ is the superficial velocity of liquid L_i and i is the integer index, that overlap and span more than six decades from 10^{-5} to 10^1 .

III. FLOW MAP

A typical flow map based on the two capillary numbers of each liquid in a pair ($G3B$: glycerol and PDMS) is displayed in Fig. 1. We find five typical regimes: (a) threading, (b) jetting, (c) dripping, (d) tubing, and (e) displacement. The threading regime corresponds to a thread that is stable over a distance $L = 20h$ (i.e., $L \gg h$) from the hydrodynamic focusing

section. The jetting regime corresponds to a thread that emits droplets at a distance $L < 20h$ from the focusing section. In microfluidic circuits, threading is clearly distinguishable from jetting, as illustrated in the “microfluidic aquarium,”⁵⁰ where capillary threads display unique morphologies. Here, when differentiating these two flow behaviors, we choose the cutoff distance to be $20h$, measured from the downstream end of the cross-channel junction, since it corresponds to the regime $L \gg h$ and is readily accessible by our typical experimental field of view. The dripping regime occurs when the cap formed by $L1$ stays in the junction after the breakup. Jetting and dripping regimes have been extensively studied for a faucet under gravity in air^{51,52} as well as in other microfluidic geometries.^{35–37} The tubing regime is mainly viscous stress controlled and corresponds to a viscous core that

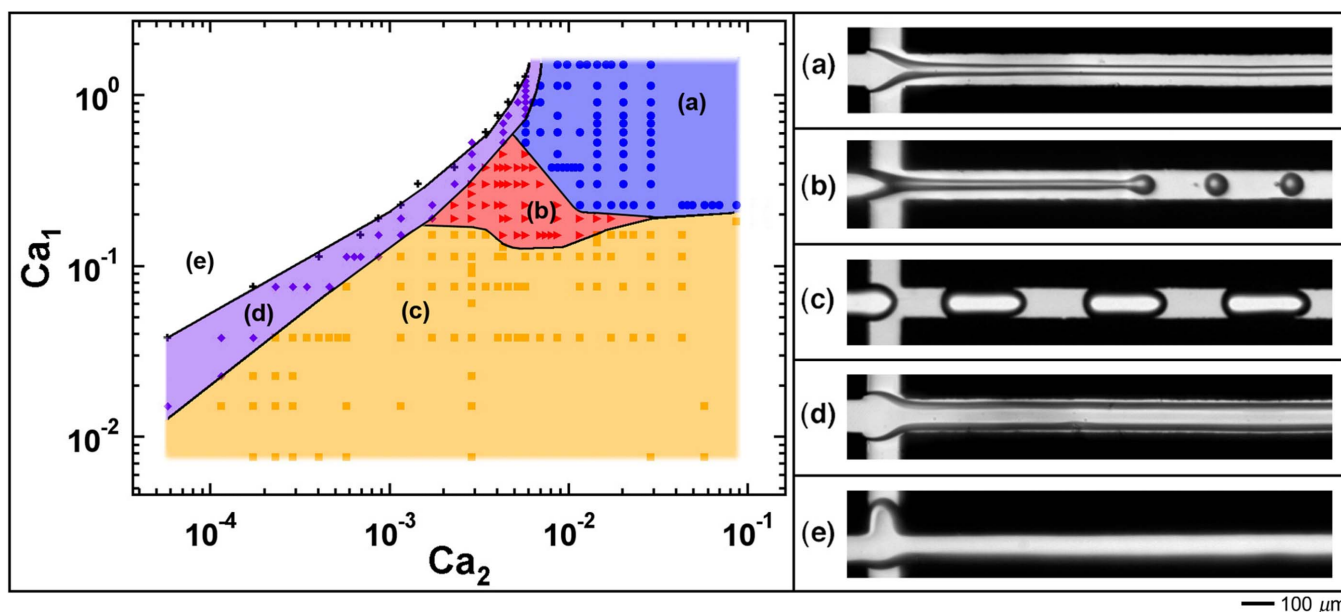


FIG. 1. (Color online) Typical capillary number-based flow map with flow patterns: (a) threading (●), (b) jetting (▶), (c) dripping (■), (d) tubing (◆), (e) viscous displacement (+), fluid pair: $G3B$.

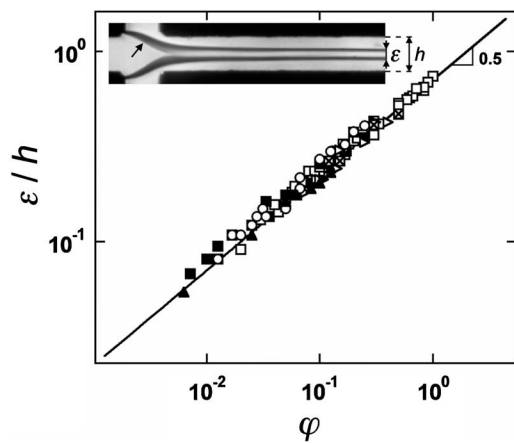


FIG. 2. Stable capillary thread diameter ε vs flow rate ratio φ . Inset: experimental micrograph with arrow showing contact line between $L1$ and $L2$ and glass wall. Fluid pairs: $G1A$ (\bullet), $G1B$ (\blacksquare), $G2B$ (\boxtimes), $G3A$ (\circ), $G3B$ (\square), and $G3D$ (\triangleright).

invades most of the cross section of the outlet channel. The displacement regime is characterized by $L1$ invading the side channels of $L2$, causing a viscous finger to form and counterflow. Although we initially attempted to produce a “universal” flow map, differences between capillary number-based transitions and viscous stress-based transitions preclude the creation of a single simple map that is valid for all pairs. We present a single representative map of the transitions in flow behavior in Fig. 1 because this map gives relatively equal importance to each regime and type of transition. After presenting this map, we focus on describing the quantitative details of the various physical processes contained within it, recognizing that the detailed location of the boundaries between different flow regimes may depend on the particular fluid system.

Relationships between multiphase regimes are typically shown on a map based on the flow rates (Q_1 , Q_2). However, in order to study the influence of physicochemical properties on the flow, we find the capillary numbers Ca_1 and Ca_2 to be more relevant. Indeed, as we independently vary each parameter J_i , η_i , and γ_{12} , over at least one order of magnitude, we find that transitions between dripping and either jetting or threading always occurs around the critical value $Ca_{1c} \approx 10^{-1}$. This value is not constant and depends on Ca_2 (Fig. 1). The idea of a critical capillary number Ca_c is conceptually very important because it quantitatively sets the cross-over between capillary-dominated flows and viscosity-dominated flows. Since $Ca_c \approx 10^{-1}$ is found in many other systems,^{35,53} observations suggest universality of this cross-over.

IV. CAPILLARY THREADS

When $Ca_1 \gg 10^{-1}$, the more viscous liquid $L1$ is focused and encapsulated by the less viscous liquid $L2$ in the center of the outlet square microchannel. In the cross itself, the contact line between $L1$ and $L2$ and the microchannel’s glass walls can be seen in Fig. 2, inset. After detaching from the walls, the $L1$ - $L2$ interface is strongly deformed before the newly formed thread reaches a constant shape after a few h .

The natural lubrication of a more viscous liquid by a less viscous one reduces viscous dissipation and is readily enhanced in microfluidics due to strong confinement. This phenomenon, specific to the large viscosity ratio $\chi = \eta_1 / \eta_2$, also occurs between miscible fluids in microfluidics,⁹ as well as in much larger systems, such as lubricated pipelining⁵⁴ or volcanic conduits.⁵⁵

A viscous thread corresponds to a core annular flow in pluglike flow that is transported by a less viscous outer coflowing fluid. In confined geometries, the case of a thread, where the more viscous fluid forms the core, significantly differs from the case of a jet, where the less viscous fluid forms the core. The flow profile for a jet is parabolic; a jet is a fast core flowing within a slower sheath. For a fixed diameter ε and a fixed sheath velocity, the peak velocity of the core decreases with the viscosity ratio χ . When $\chi > 15$, the core reaches an asymptotic regime,⁹ which corresponds to a thread, with a nearly flat velocity profile. Therefore, a viscous thread is transported or extruded by the less viscous fluid flowing outside.

In Fig. 2, we present measurements of the stable thread diameter ε as a function of the flow rate ratio, $\varphi = Q_1 / Q_2$, for pairs in each group. We find the following relationship:

$$\frac{\varepsilon}{h} \approx \left(\frac{Q_1}{2Q_2} \right)^{1/2}. \quad (1)$$

Since ε does not depend on the viscosities, there is strong evidence that the thread of $L1$ is completely surrounded (i.e., lubricated) by $L2$. Since ε is also independent of γ_{12} , the regime is purely viscous. The scaling in Eq. (1) corresponds to the asymptotic solution of a small cylindrical thread ($\varepsilon \ll 1$) in a circular tube which has been analytically derived by simply neglecting γ_{12} in the stress balance at the interface, similar to miscible fluids when diffusion is neglected.⁵⁶ Our measured scaling extends its range of validity to square channels with no additional prefactor and up to $\varepsilon < 0.8h$. Since velocity lines in a square channel are quasicircular in the duct center,⁵⁷ thin threads far away from the cross channel are assumed to have a circular cross section and flow with a spatially constant velocity, estimated by using Eq. (1) by $U_1 \approx 4Q_1 / (\pi\varepsilon^2) \approx 8Q_2 / (\pi h^2)$. This important information about the velocity field has not been available in previous thread experiments.⁵⁸ In summary, for “high” capillary numbers, $Ca_1 \gg 10^{-1}$, interfacial tension can be neglected, and the lubricated thread configuration is equivalent to the two-fluid primary flow.

V. JETTING

We observe that threads formed from all immiscible liquid pairs that we have studied undergo a capillary instability for $Ca_1 > 10^{-1}$. The growth of axisymmetric varicose deformations ultimately causes the thread to break up into an array of droplets.⁵⁸ In order for varicose deformations to naturally grow, the thread must assume a small shape for wall effects to be neglected. Figure 3 displays experimental micrographs of the jetting instability for the fluid pair $G3C$. The

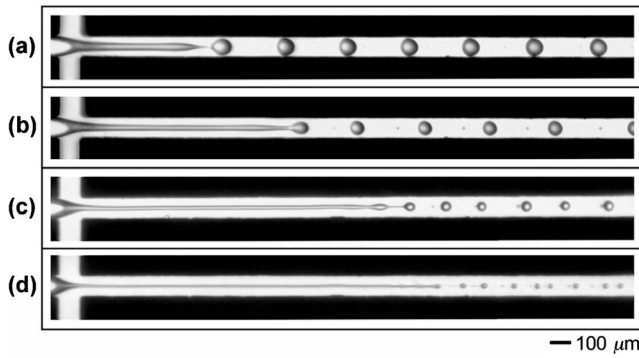


FIG. 3. Jetting regime. Thread breakup location occurs near fluid junction and is adjusted with flow rates in $\mu\text{l}/\text{min}$: (a) $Q_1=1$, $Q_2=4$; (b) $Q_1=1$, $Q_2=8$; (c) $Q_1=1$, $Q_2=14$; (d) $Q_1=0.6$, $Q_2=40$ (fluid pair: G3C).

critical thread length L_C before jetting occurs can be adjusted with the flow rates (Q_1 , Q_2), which control the time scale of the flow.

A. Droplet diameter

For pairs in each group, we measure the droplet diameter d from the micrographs as function of Q_1 , Q_2 , η_1 , η_2 , and γ_{12} . We find that d collapses on a single master curve which depends only on the flow rate ratio $\varphi=Q_1/Q_2$ (Fig. 4),

$$\frac{d}{h} \approx 3.1 \left(\frac{Q_1}{2Q_2} \right)^{1/2}. \quad (2)$$

In some cases, bidispersity is observed, and the reported value of d represents the average diameter. If tiny satellite droplets are created, then we report only d of the much larger “mother” droplet. The functional form of d is identical to that of ε for a stable thread [Eq. (1)], i.e., proportional to $\varphi^{1/2}$. From the micrographs, we measure ε and find a constant value of $d/\varepsilon=2.9 \pm 0.3$ (Fig. 4, inset). Despite the short length of the thread, the local stable ε in the jetting regime is only in small excess of $(\varphi/2)^{1/2}$. The scaling in Eq. (2) appears to be robust until $d/h \approx 3$. In the case $d > h$, the droplets are elongated, and we measure d as being the droplet length along the channel. The transition between spherical and elongated droplets is smooth in the jetting regime. From Eq. (2), the regime of formation of subchannel droplet sizes, $d/h < 1$, is achieved when $\varphi < \varphi_c$, where $\varphi_c \approx 0.21$ is a critical flow rate ratio.

B. Mode of maximum instability

Over the range of parameters investigated, the droplets remain quasispherical and the volume of satellite droplets is typically negligible compared to the volume of a mother drop. Therefore, the threads’ mode of maximum thread instability, $x=\pi\varepsilon/\lambda$, where λ is the most unstable wavelength, can be estimated by comparing the volume of a droplet, $V_d=\pi d^3/6$, to the volume of a thread of length λ , $V_t=\lambda\pi\varepsilon^2/4$. Since $d/\varepsilon \approx 2.9$, we find that $x \approx 0.19 \pm 0.06$. According to linear stability analysis,² the mode of maximum instability of a water jet is $x=0.697$, which correspond to Rayleigh’s optimal wavelength, $\lambda \approx 9(\varepsilon/2)$. A shift toward smaller x is

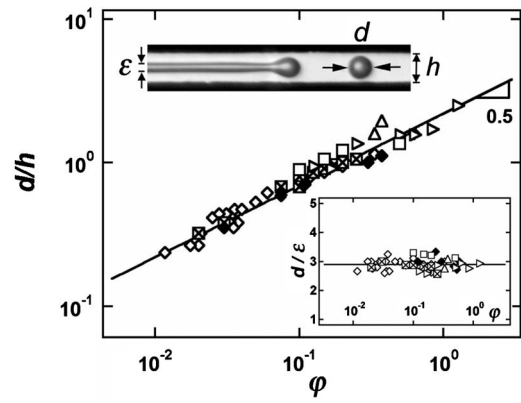


FIG. 4. Normalized jetting droplet diameter d vs the flow rate ratio φ . Solid line: $d=3.1(\varphi/2)^{1/2}$. Inset: ratio d/ε vs φ . Solid line: $d/\varepsilon=2.9$. Fluid pairs: G1C (\blacklozenge), G2B (\boxtimes), G3B (\square), G3C (\diamond), G3D (\triangleright), G3E (\triangle).

expected when the liquid viscosity increases. For the case of a thread surrounded by another viscous liquid, Tomotika⁵⁹ calculated that x takes a maximum of 0.589 when $\chi=0.28$ and monotonically decreases with χ . Examples of these calculations include $x=0.353$ when $\chi=20$ and $x=0.243$ when $\chi=100$. When the core viscosity is paramount ($\chi \rightarrow \infty$), theory predicts that there is no finite mode of maximum instability,^{2,59–61} i.e., $x=0$. This theoretical result is in good agreement with the observed behavior of stable falling viscous threads⁶² stretched by gravity. Here, for a confined thread flowing at constant velocity and χ ranging between 22 and 1484, experimental results show that the mode of maximum instability saturates around $x \approx 0.19$. This situation considerably differs from Tomotika’s calculations, which were performed, however, under the supposition that there were no general flows in both fluids. Therefore, solving the relationship between the mode of maximum instability x and the viscosity contrast χ in the presence of shear in the environment would provide further insights on the behavior of lubricated viscous microthreads.

C. Critical thread length

In the square microchannels, the viscous flow is strongly laminar and fully developed [$\text{Re}_i \ll 1$, where the Reynolds number $\text{Re}_i = \rho_i Q_i / (\eta_i h)$, with ρ_i being the density associated with Li], so inertia is not relevant. In this type of flow, the time scale over which a viscous thread becomes unstable should scale with the capillary time:⁵⁸ $t_c \propto \varepsilon \eta_1 / \gamma_{12}$. However, this time scale assumes that the crossover between capillary and viscous flows occurs for $\text{Ca}=1$. A more realistic estimate for the viscous-capillary time is $T_c \approx t_c / \text{Ca}_c$. For $\text{Ca}_1 > \text{Ca}_c$, the instability is convective,⁶³ varicose perturbations develop near the focusing section and are subsequently advected with the flow. Under these conditions, the critical thread length is expected to be $L_c \approx U_1 T_c$. According to the two-fluid primary flow, the thread velocity is $U_1 \approx 8Q_2 / (\pi h^2)$, which gives

$$L_c = C_j \frac{\eta_1}{\gamma_{12}} \frac{8}{\pi h \text{Ca}_c} \left(\frac{Q_1 Q_2}{2} \right)^{1/2}, \quad (3)$$

where C_j is a numerical constant close to unity. For each fluid pair, we measure $L_{c,\text{exp}}$ and compare to the predicted L_c

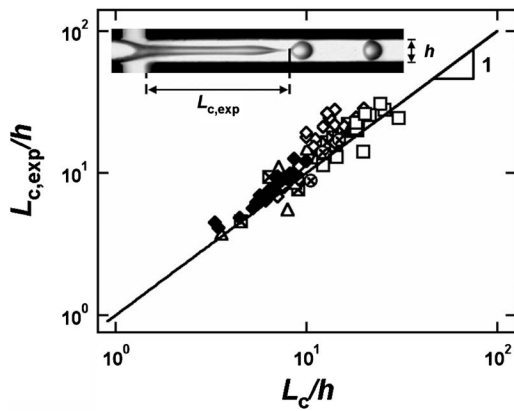


FIG. 5. Experimental critical thread length $L_{c,exp}$ before jetting droplets compared to the prediction of Eq. (3) (solid line). Fluid pairs: $G1C$ (\blacklozenge), $G1D$ (\blacktriangle), $G2A$ (\otimes), $G2B$ (\boxtimes), $G3B$ (\square), $G3C$ (\diamond), and $G3E$ (\triangle).

for $C_j=2.1$ and $Ca_c=10^{-1}$ (Fig. 5). Although the experimental results are somewhat scattered, the agreement is reasonably good, since the ratio η_1/γ_{12} spans over two decades between pairs $G1D$ and $G3E$. In order to obtain comparable L_c for these pairs, we compensate η_1/γ_{12} by adjusting Q_1 and Q_2 . At least some of the scatter may result from the assumption that the thread diameter linearly decreases with time and that nonlinear behaviors^{58,61} near breakup are neglected. However, we observe no systematic trend or departure that depends on the viscosity ratio. Here, the outer viscosity η_2 , which is varied by a factor of 61, does not seem to be relevant in the process. We find it to be conceptually interesting that L_c is proportional to the geometric means of the flow rates $L_c \propto (Q_1 Q_2)^{1/2}$, which explains the shape of the transition from jetting to threading on the flow map (Fig. 1).

D. Varicose confinement

When threads are thick ($\varphi > \varphi_c$), varicose deformations arising from the capillary instability are affected by the presence of the walls, which provide geometrical confinement.^{64,65} Although the thread is free to thin at the nodes, it cannot grow beyond the channel width h at the antinodes. As a result, jetting creates complex patterns due to the difference in drag caused by the obstruction of the channel flow at the antinodes and the peak velocity at the node. The natural wave propagation along the viscous core is perturbed and L_c becomes nonsteady. Examples of varicose confinement are given in Fig. 6. Near φ_c , the system presents the same morphology as the coating instability of a rigid fiber⁶⁶ in which multiple pinch-off points are regularly spaced along the thread [Fig. 6(a)]. This beads-on-a-string structure is typical of viscoelastic jets,⁶⁷ such as polymer solutions.⁶⁸ For larger φ , the system approaches the tubing transition and capillary waves can travel farther in the channel leading to bamboo waves.⁵⁴

VI. DRIPPING

Dripping is characterized by elongated droplets of length d , which are typically larger than h . We find dripping to steadily occur for $Ca_1 < 10^{-1}$ and for $Ca_2 < 10^{-1}$. Perturba-

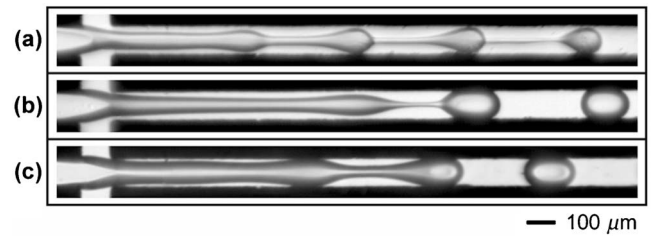


FIG. 6. Examples of microchannel confinement of varicose deformations (flow rates in $\mu\text{l}/\text{min}$): (a) Bead-on-a-string structure: $Q_1=4$, $Q_2=40$ ($G2A$); (b) $Q_1=3$, $Q_2=6$ ($G3B$); (c) $Q_1=10$, $Q_2=16$ ($G3D$).

tions caused by γ_{12} stay in the reference frame of the cross, and the breakup process shows the features of an absolute instability.⁶³ However, contrary to jetting, dripping created by cross flows is not a free, self-driven breakup phenomenon since it is largely dictated by flow rates and geometry.

A. Dynamics

Droplet formation by dripping can be divided into five distinct stages. The first stage corresponds to the displacement of a quasispherical cap formed by $L1$ in the cross [between (i) and (ii) in Fig. 7(a)]. Since $L1$ is supplied at Q_1 , the initial cap velocity is $J_1=Q_1/h^2$ and it is slightly accelerated by $L2$ in the cross [Fig. 7(c)]. When the cap reaches the edge of the outlet channel, the flow path of $L2$ becomes significantly obstructed,^{34,69} and $L2$ squeezes $L1$, which experiences a large acceleration before its plateaus near the multiphase superficial velocity, $J=J_1+J_2$, at the end of the second stage [between (ii) and (iii) in Fig. 7(a)]. In the pinching stage (iii)–(iv), $L2$ works against interfacial tension γ_{12} to thin the neck between the main droplet and the matrix. For $Ca_1 \ll 10^{-1}$, final breakup occurs at the end of the pinching stage. The fourth stage occurs at the onset of the viscous regime ($Ca \sim 10^{-1}$): the droplet pulls a thin viscous tail out of the $L1$ matrix (v). The eventual breakup of the tail, which gives birth to satellite droplets, completes the main cycle (v)–(vi). Since satellite droplets are dragged along by the flow near the peak velocity in the channel center, they soon catch up with the mother droplet, as can be seen on the time-space diagram in Fig. 7(b). The tendency for small droplets to flow faster than larger ones extends over $d > h$. However, due to the importance of the open corners in a square channel, dissipation in the films between the droplet and the walls is not predominant, and elongated droplets flow near the mixture velocity J [Figs. 7(c) and 7(d)].

B. Droplet length

The main droplet length d is determined during the pinching stage. By assuming a constant droplet velocity, $U_d \approx J=(Q_1+Q_2)/h^2$, d can be estimated to be $d \approx JT_{pinch}$, similar to bubble formation in the same geometry.²⁰ However, since $L1$ cannot become a compressible jet, $T_{pinch} \gg T_2=h^3/Q_2$, where T_2 is the time scale of the flow of $L2$. For $\chi \geq 22$, we experimentally find that d weakly depends on η_1 , which we have varied by a factor of 24, yet d strongly depends on η_2 and γ_{12} . Since $L1$ has a nearly flat velocity

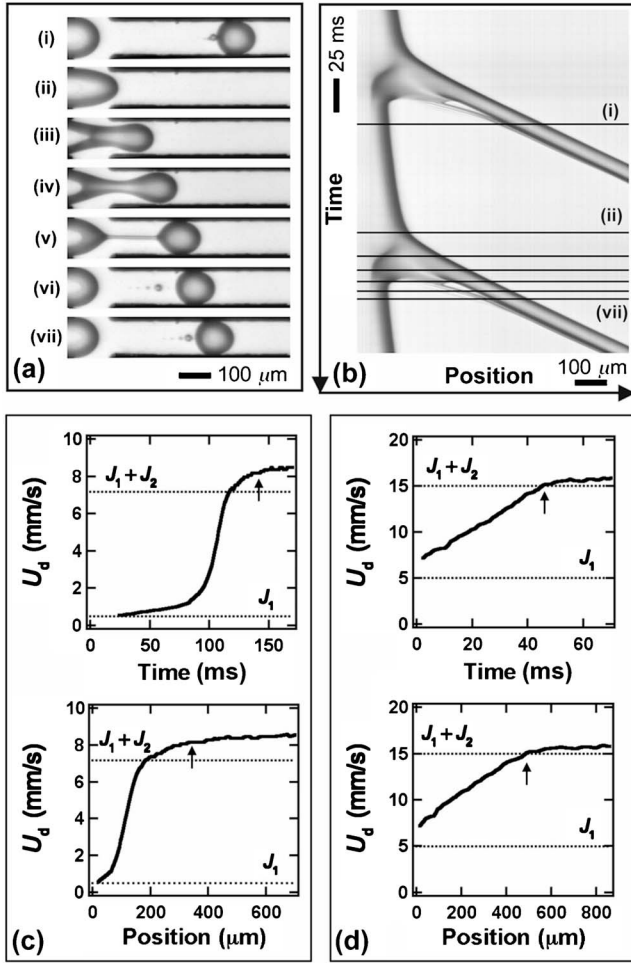


FIG. 7. Dynamics of dripping: (a) Time series of a cycle of viscous droplet formation: (i)–(ii) cap displacement, (ii)–(iii) cap squeezing, (iii)–(iv) pinching, (v) tail stretching, and (vi)–(vii) complete breakup. (b) Time-space diagram of (a) with corresponding events taken along the centerline of the channel. (c) Front velocity of a small droplet, $d/h \approx 1.16$, during breakup (flow rates in $\mu\text{l}/\text{min}$): $Q_1=0.3$, $Q_2=4$ (fluids pair: G3C). (d) Front velocity of a large droplet, $d/h \approx 2.48$, during breakup: $Q_1=3$, $Q_2=6$ (fluids pair: G3D). The arrow indicates the end of the pinching stage.

profile and is lubricated by $L2$ at the imposed flow rate Q_2 , η_1 is not relevant in this process. The stretching of the neck creates more interfacial area between $L1$ and $L2$. As a result, γ_{12} acts against droplet formation in the dripping regime. On the contrary, γ_{12} acts in favor of droplet formation in the jetting regime because the interfacial area of a thread is reduced through spatially free varicose deformations. Based on these insights, we estimate $T_{\text{pinch}} \approx T_2/\text{Ca}_2$ since T_{pinch} is expected to be proportional to T_2 and inversely proportional to the ratio of viscous to capillary effects on the flow: Ca_2 . By using the volume fraction of $L2$, $\alpha_2=Q_2/(Q_1+Q_2)$, we find the following simplified scaling: $d \propto (\alpha_2 \text{Ca}_2)^{-1}$. In Fig. 8, we measure d/h as a function of $\alpha_2 \text{Ca}_2$, and, for all fluid pairs, d collapses on a single master curve. Although the data for d/h continuously decrease as $\alpha_2 \text{Ca}_2$ increases, we empirically identify and define two regions of qualitatively different behaviors on opposite sides of a cutoff value of $d_c/h \approx 2.5$,

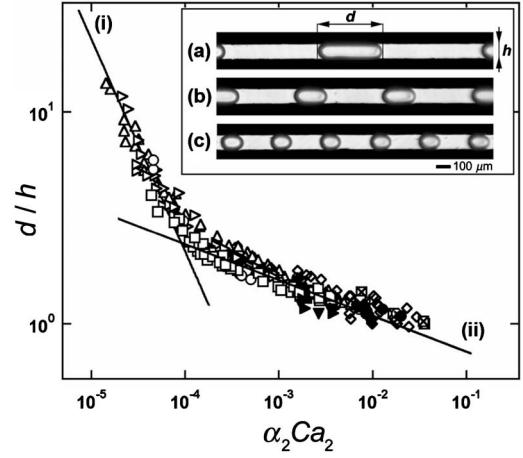


FIG. 8. Normalized droplet length d/h vs $\alpha_2 \text{Ca}_2$. Line (i): $d/h = 2.2 \times 10^{-3} (\alpha_2 \text{Ca}_2)^{-1}$, line (ii): $d/h = 0.5 (\alpha_2 \text{Ca}_2)^{-0.17}$. Fluids pairs: G1A (●), G1C (◆), G1D (▲), G1E (▶), G2A (⊗), G2B (⊠), G3A (○), G3B (○), G3C (◇), G3D (▷), and G3E (△). Inset: effect of Ca_2 for fixed volume fraction: $\alpha_2=2/3$ (flow rates in $\mu\text{l}/\text{min}$) (a) $Q_1=1$, $Q_2=2$; (b) $Q_1=5$, $Q_2=10$; (c) $Q_1=25$, $Q_2=50$ (fluid pair: G3E).

$$\frac{d}{h} \approx \begin{cases} 2.2 \times 10^{-3} (\alpha_2 \text{Ca}_2)^{-1} & \text{for } d > 2.5h \\ 0.5 (\alpha_2 \text{Ca}_2)^{-0.17} & \text{for } d < 2.5h. \end{cases} \quad (4)$$

It is worth noting that the scaling based on $\alpha_2 \text{Ca}_2$ does not rescale the data on a single master curve when $\chi < 15$. For brevity, for the remainder of this discussion, we consider only the experimental data for $\chi \geq 22$. Each region in Eq. (4) presents some expected and unexpected features. For $d > 2.5h$, the exponent of -1 can be deduced from the simple analysis above, but the origin of the extremely small factor of 2.2×10^{-3} is not yet well understood. For $d < 2.5h$, the factor of 0.5 is on the order of unity. In this region, the exponent of -0.17 can be qualitatively understood by arguing that small droplets present more resistance to side flow-induced breakup (due to the relatively large increase of interfacial area) and that the influence of squeezing stage cannot be neglected as $d \rightarrow h$. The dependency of d on Ca_2 is illustrated in Fig. 8, inset, where $\alpha_2=0.66$ is fixed. Since α_2 is constant, the volumes of $L1$ and $L2$ are the same in these three images, and Ca_2 increases by a factor of 5 . When displayed this way, from (a) to (c), each droplet from an upper image appears to be divided into two droplets in the image immediately below it.

C. Viscous tail

When Ca_1 approaches 10^{-1} , we observe the persistence of a tail,^{70,71} which connects the droplet to the continuous phase of $L1$ in the inlet channel and cross. When the tail becomes thin enough, it breaks into an array of satellite droplets, the size and distribution of which depend on the length of the tail at breakup, l_c . The tail is clearly reminiscent of the primary flow: at the transition to jetting and threading, a small increase in Ca_1 stabilizes the tail, which then matures into a locally stable thread. As a droplet of $L1$ emerges and begins to move downstream, it pulls out a tail and remains connected to the liquid $L1$ in the inlet channel. The liquid $L1$ is flowing in the tail and is feeding the droplet from its ma-

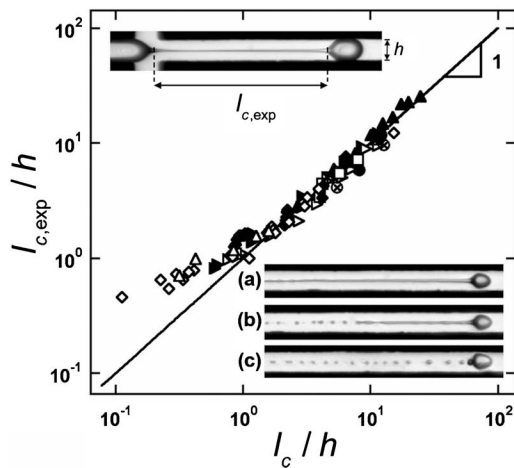


FIG. 9. Critical tail length at breakup, l_c , of a viscous droplet vs Eq. (5). Fluids: *G1A* (●), *G1C* (◆), *G1D* (▲), *G1E* (►), *G2A* (⊗), *G2B* (⊠), *G3B* (⊞), *G3D* (▷), and *G3E* (△). Inset: Example of cometlike droplets with long tails (flow rates in $\mu\text{l}/\text{min}$): [(a) and (b)] $Q_1=0.5$, $Q_2=40$; (c) $Q_1=0.6$, $Q_2=40$ (fluids pair: *G3C*).

matrix in the cross channel. To some extent, the tail is analogous to an umbilical cord linking the matrix to the droplet. However, droplets with long tails also resemble comets (Fig. 9, inset) from which satellites are formed, which suggests a celestial analogy. For a constant droplet velocity, $U_d \approx J$, the length of the tail at breakup, l_c , is estimated by $l_c \approx JT_{c,t}$, where $T_{c,t} = \eta_1 h / (\gamma_{12} \text{Ca}_c)$ is the critical capillary time associated with the tail. Here, $h/2$ is arbitrarily chosen instead of ε because the tail is continuously thinning after the pinching stage without reaching a stable configuration. The previous argument gives

$$\frac{l_c}{h} = C_t \frac{\eta_1}{\gamma_{12} \text{Ca}_c} \frac{Q_1 + Q_2}{2h^2}, \quad (5)$$

where C_t is a numerical constant close to unity. In Fig. 9, we measure $l_{c,\text{exp}}$ for each fluid pair and find an excellent agreement with $l_c > h$ for $C_t = 1.0$ and $\text{Ca}_c = 10^{-1}$. It is remarkable that C_t is essentially unity despite the complexity of the phenomenon and the simplicity of our scaling argument. For relatively low Ca_1 , tail breakup occurs at the tip of the matrix of *L1* in the cross. When $\text{Ca}_1 \sim \text{Ca}_c$, some interfacial pertur-

bations are convected along with the first breakup location. Characteristic to capillary breakup in a viscous environment, the shape of the tail resembles a double cone on either side of the pinching region.^{72,73} The development of the perturbations and the pinching location strongly affect the size and the distribution of satellite droplets. The dynamics of satellite droplet formation is particularly interesting for producing tiny droplets; it is strongly affected by the presence of surfactant.³⁵ In our case, a large number of satellite droplets are produced for long tails (Fig. 9, inset). A part of the tail can recede back into the main droplet or the matrix. Persistent viscous tails are also observed in the jetting regime, which introduce some fluctuations in the jetting location. On contrary, in the dripping regime, the tail is linked to a spatially fixed matrix and satellite droplet production is steadier.

VII. TUBING, DISPLACEMENT, AND WETTING

A. Tubing

Several other physical properties can affect the formation of threads and droplets. The threading, jetting, and dripping regimes are bounded by the tubing regime [Fig. 10(a)]. Tubing occurs when the viscous stress, $\tau_1 = \eta_1 Q_1 / h^3$, associated with the flow of *L1*, is comparable to the viscous stress, $\tau_2 = \eta_2 Q_2 / h^3$, associated with the flow of *L2*. This regime corresponds to filling almost the entire outlet channel's cross section with *L1*. In this case, the viscous flow of the core liquid cannot be assumed to be circular but rather square with rounded corners. Tubing is analogous to “dry flow” that has been observed by using liquid/gas pairs¹⁸ in square microchannels. Dry flow is characterized by a local drying of the walls by the gas, which creates steady contact lines that are parallel to the flow. Tubing is the result of a lubrication failure of *L1* by *L2*, which flows nearly entirely in the corners of the square microchannels. We experimentally observe that this regime is hysteretic. For instance, at the tubing/threading transition, the two regimes exist for the same input parameters depending on the history of the system. When φ is increased from the displacement regime [Fig. 10(b)], tubing is persistent; when φ is decreased from the threading regime, the lubricated thread remains persistent. These observations suggest a transition between the wetting of the

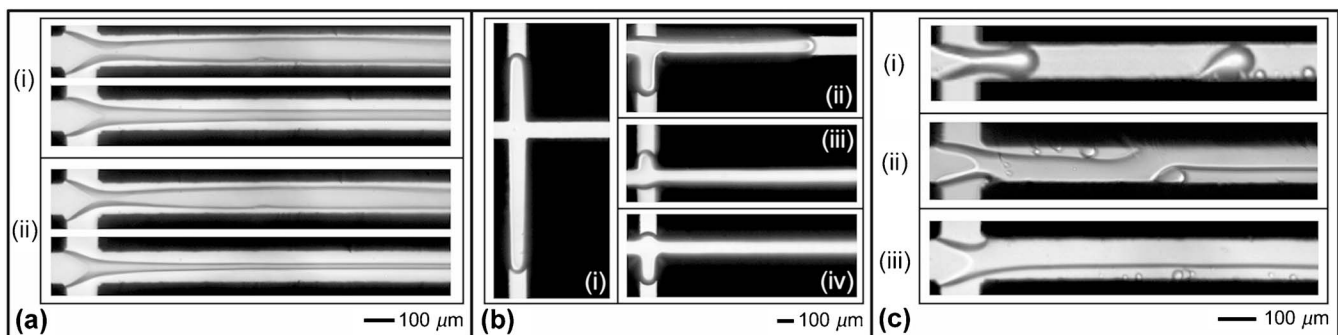


FIG. 10. Examples of flow regimes limiting the steady formation of threads and droplets: (a) Hysteresis between tubing and threading regimes (flow rates in $\mu\text{l}/\text{min}$): (i) $Q_1=0.5$, and $Q_2=4$, (ii) $Q_1=0.5$, $Q_2=10$ and (fluid pair: *G1A*). (b) Viscous displacement regime (finger of *L2* at counterflow with *L3*): (i) $Q_1=8$, $Q_2=10$, (ii) $Q_1=1$, $Q_2=1.6$, (iii) $Q_1=0.3$, $Q_2=0.2$ (*G3B*), (iv) $Q_1=1$ and, $Q_2=0.4$ (*G3D*). (c) Typical wetting behaviors: (i) sticking droplet, $Q_1=0.1$, $Q_2=1$ (*G1D*); stratification: (ii), $Q_1=0.2$, $Q_2=2$ (iii) $Q_1=0.2$, $Q_2=1$ (*G1B*).

walls with $L1$ and $L2$. For a given fluid pair, tubing is a steady state that can be achieved by controlling the flow history.

B. Displacement

By contrast to steady tubing, unsteady states are reached when $\tau_1 \gg \tau_2$. In this situation, the viscous displacement regime is characterized by $L1$ invading at least one of the two side channels into which $L2$ is injected at the intersection of the cross [Fig. 10(b)]. This situation is an unsteady state since the invading fingers are eventually pushed back into the outlet channel, which creates a complex loop due to the constant mass flux imposed by the syringe pumps. As a result of the viscous counterflow, asymmetrical growth into side channels is usually observed, even though both side channels are each independently fed with $L2$ at $Q_2/2$. The other displacement regime, which corresponds to $L2$ invading the inlet channel of $L1$, is reached when $\tau_1 \ll \tau_2$. These fluid switching regimes are potentially interesting to study as self-regulated microsystems that may be useful for chemical reactions.

C. Wetting

Threads and droplet formation are steady when $L1$ does not wet the walls of the outlet channel, i.e., when $\theta_{1a} \rightarrow \pi$, where θ_{1a} is the advancing contact angle inside the droplet ($L1$) and the solid wall. This situation is achieved when the receding contact angle of the liquid matrix ($L2$) on the walls θ_{2r} , where $\theta_{2r} = \pi - \theta_{1a}$, approaches zero. For partially wetting liquids, this situation is met for a critical Ca_d , above which a translating liquid can coat a solid surface with a film,⁷⁴ by analogy, translating droplets can leave satellite droplets behind on the solid surface as well.⁷⁵ In our system, Ca_d plays a major role for small γ_{12} ($G1$). Indeed, small interfacial tensions γ_{12} are obtained between liquids with comparable surface tensions γ , such as silicone oil and alcohol. Since $L1$ and $L2$ similarly wet solids, a partially wetting system is formed when they make contact at a solid wall ($\theta_1 \sim \theta_2 \sim \pi/2$, where θ is the static contact). For fluids in group $G1$, we observe wetting flows when $Ca_1 < Ca_d \approx 10^{-2}$. The large range of behaviors associated with wetting phenomena has been long identified as a field in itself.⁷⁶ In our system, the presence of the contact lines induces a competition between wetting and lubricating effects. When a droplet sticks to the walls, it may leave small droplets of higher curvature on the walls. These droplets could then be collected by the front of the next droplet, e.g., (i) in Fig. 10(c). The wetting of the walls by the thread typically results in the formation of a stratification, the shape of which is hysteretic, e.g., (ii) and (iii) in Fig. 10(c). In the presence of surfactant and surface modifications, numerous other wetting regimes have been reported for micro-two-phase flows.^{15,77}

VIII. CONCLUSION

We have investigated the formation of viscous threads and droplets of pairs of immiscible liquids injected in a highly symmetric hydrodynamic focusing geometry com-

prised of straight microchannels that have square cross sections. By performing a comprehensive investigation that covers a large range of fluid properties and flow rates, we have examined a variety of flow behaviors associated with large viscosity contrasts. In particular, despite the complexity of the system, we deduce empirical laws [Eqs. (1)–(5)] that can be at least qualitatively understood using simple, yet reasonable, physical arguments. For large viscosity contrasts, we have clarified the role of the inner and outer viscosities, as well as the effects of capillarity, on multiphase flows in square microchannels. For $Ca_1 \gg Ca_c$, we show that the formation of capillary threads depends only on the flow rate ratio φ . This situation characterizes the two-fluid primary flow in the system. The identification of primary flow is an advantage that allows us to deduce the expression for the critical thread length L_c before jetting. Jetting allows for the production of subchannel size droplets, the size of which depends only on φ . In addition, we demonstrate that the mode of maximum instability of a confined viscous threads flowing at constant velocity saturates at a fixed value $x = 0.19$. We investigate the dynamics of the dripping regime, and we find that the key dimensionless parameter $\alpha_2 Ca_2$ allows us to rescale the droplet size produced by using all fluid pairs onto a master curve. In the dripping regime, we show that the droplet length does not depend on η_1 . We investigate the persistence and the critical length l_c of a viscous tail that gives rise to satellite droplets. Finally, we briefly describe the regimes that limit the formation of threads and droplets. This study provides a means for producing supra- and subchannel size viscous droplets through a variety of mechanisms resulting from continuous flows.

From a practical point of view, this investigation shows that viscous droplet and thread formation strongly depend on the values of capillary number for each phase Ca_1 and Ca_2 compared to the critical capillary, $Ca_c \approx 10^{-1}$, at which viscous and capillary stresses balance. Below Ca_c , the dripping regime allows for creating monodisperse arrays of suprachannel size droplets. Near Ca_c , slender viscous structures become persistent and a viscous tails appear behind dripping droplets. The breakup of the tail produces complex arrays of satellite droplets, the typical size of which is below the channel size h . The resulting flow pattern is composed of suprachannel size droplets, i.e., dripping droplets, and subchannel size droplets, i.e., satellite droplets. Above Ca_c , the jetting regime occurs and allows for steadily producing subchannel size droplets at adjustable locations. Compared to the dripping regime with viscous tails, the jetting regime is advantageous for forming small droplets with a high rate of production and in the absence of large droplets. When $Ca_1 \gg Ca_c$, the threading regime occurs. The continuous formation of viscous capillary objects can be hindered by wetting (small flow rates) as well as by tubing and displacement (large flow rate ratios). These results are obtained by using a universal hydrodynamic focusing geometry into a square outlet channel with straight walls. This geometry is characterized by only one length scale h and significantly differs from a flow-focusing geometry, which includes a constriction at the entrance of the outlet channel. Here, in the absence of defocusing effects downstream from a constriction, a study

of the influence of fluid and flow properties on droplet and slender viscous structure formation in a square microchannel is presented.

Our study of the microfluidic confinement of capillary threads and viscous droplets with Newtonian fluids provides a basis for studying flow behavior with viscous industrial and biological fluids. This suggests that viscous complex fluids such as non-Newtonian polymeric fluids, nanoemulsions, concentrated surfactant solutions, or gels could be precisely manipulated with reactive solvent in microfluidic devices. The understanding of the asymptotical behaviors associated with flow of viscous fluid pairs in simple geometries also provides a solid foundation and a framework for unraveling the various microtransport phenomena in complex and natural geometries.

ACKNOWLEDGMENTS

We wish to thank Jung-Ren Huang for helping with measurements of interfacial tensions. We have enjoyed discussions with Thomas Ward. This work was supported in part by the McTague Chair at UCLA.

¹G. K. Batchelor, *An Introduction to Fluid Mechanics* (Cambridge University Press, New York, 1967).

²S. Chandrasekhar, *Hydrodynamic and Hydromagnetic Stability* (Dover, New York, 1981).

³G. I. Taylor, "The formation of emulsions in definable fields of flow," *Proc. R. Soc. London, Ser. A* **146**, 501 (1934).

⁴J. M. Rallison, "The deformation of small viscous drops and bubbles in shear flows," *Annu. Rev. Fluid Mech.* **16**, 45 (1984).

⁵J. Bibette, F. Leal-Calderon, and P. Poulin, "Emulsions: Basic principles," *Rep. Prog. Phys.* **62**, 969 (1999).

⁶T. G. Mason and J. Bibette, "Emulsification in viscoelastic media," *Phys. Rev. Lett.* **77**, 3481 (1996).

⁷C. D. Eggleton, T.-M. Tsai, and K. J. Stebe, "Tip streaming from a drop in the presence of surfactants," *Phys. Rev. Lett.* **87**, 048302 (2001).

⁸J. M. Fernandez and G. M. Homsy, "Chemical reaction-driven tip streaming phenomena in a pendant drop," *Phys. Fluids* **16**, 2548 (2004).

⁹T. Cubaud and T. G. Mason, "Folding of viscous threads in diverging microchannels," *Phys. Rev. Lett.* **96**, 114501 (2006).

¹⁰T. Cubaud and T. G. Mason, "Swirling of viscous fluid threads in microchannels," *Phys. Rev. Lett.* **98**, 264501 (2007).

¹¹C.-M. Ho and Y.-C. Tai, "Micro-electro-mechanical systems (MEMS) and fluid flows," *Annu. Rev. Fluid Mech.* **30**, 579 (1998).

¹²T. M. Squires and S. R. Quake, "Microfluidics: fluid physics at the nanoliter scale," *Rev. Mod. Phys.* **77**, 977 (2005).

¹³H. A. Stone, A. D. Stroock, and A. Ajdari, "Engineering flows in small devices: microfluidics toward a lab-on-a-chip," *Annu. Rev. Fluid Mech.* **2004**, 381 (2004).

¹⁴T. Thorsen, R. W. Roberts, F. H. Arnold, and S. R. Quake, "Dynamic pattern formation in a vesicle-generating microfluidic device," *Phys. Rev. Lett.* **86**, 4163 (2001).

¹⁵R. Dreyfus, P. Tabeling, and H. Willaime, "Ordered and disordered patterns in two-phase flows in microchannels," *Phys. Rev. Lett.* **90**, 144505 (2003).

¹⁶G. Hestroni, A. Mosyak, Z. Segal, and E. Pogrebnyak, "Two-phase flow patterns in parallel micro-channels," *Int. J. Multiphase Flow* **29**, 341 (2003).

¹⁷D. R. Link, S. L. Anna, D. A. Weitz, and H. A. Stone, "Geometrically mediated breakup of drops in microfluidic devices," *Phys. Rev. Lett.* **92**, 054503 (2004).

¹⁸T. Cubaud and C.-M. Ho, "Transport of bubbles in square microchannels," *Phys. Fluids* **16**, 4575 (2004).

¹⁹W. Engl, M. Roche, A. Colin, P. Panizza, and A. Ajdari, "Droplet traffic at a simple junction at low capillary numbers," *Phys. Rev. Lett.* **95**, 208304 (2005).

²⁰T. Cubaud, M. Tatini, X. Zhong, and C.-M. Ho, "Bubble dispenser in microfluidic devices," *Phys. Rev. E* **72**, 037302 (2005).

²¹J. T. Cabral and S. D. Hudson, "Microfluidic approach for rapid multicomponent interfacial tensiometry," *Lab Chip* **6**, 427 (2006).

²²L. Ménétrier-Deremble and P. Tabeling, "Droplet breakup in microfluidic junctions of arbitrary angles," *Phys. Rev. E* **74**, 035303 (2006).

²³T. Kawakatsu, H. Komori, M. Nakajima, Y. Kikuchi, and T. Yonemoto, "Production of monodisperse oil-in-water emulsion using cross flow-type silicon microchannel plate," *J. Chem. Eng. Jpn.* **32**, 241 (1999).

²⁴S. Sugiura, M. Nakajima, S. Iwamoto, and M. Seki, "Interfacial tension driven monodispersed droplet formation from microfabricated channel array," *Langmuir* **17**, 5562 (2001).

²⁵S. Sugiura, M. Nakajima, T. Oda, and M. Seki, "Effect of interfacial tension on the dynamic behavior of droplet formation during microchannel emulsification," *J. Colloid Interface Sci.* **269**, 178 (2004).

²⁶T. Nisisako, T. Torii, and T. Higuchi, "Droplet formation in a microchannel network," *Lab Chip* **2**, 24 (2002).

²⁷J. D. Tice, H. Song, A. D. Lyon, and R. F. Ismagilov, "Formation of droplets and mixing in multiphase microfluidics at low values of the Reynolds and the capillary numbers," *Langmuir* **19**, 9127 (2003).

²⁸P. Garstecki, M. Fuerstman, H. A. Stone, and G. W. Whitesides, "Formation of droplets and bubbles in a microfluidic T-junction—scaling and mechanism of breakup," *Lab Chip* **6**, 437 (2006).

²⁹J. H. Xu, G. S. Luo, S. W. Li, and G. G. Chen, "Shear force induced monodisperse droplet formation in a microfluidic device by controlling wetting properties," *Lab Chip* **6**, 131 (2006).

³⁰Q. Xu and M. Nakajima, "The generation of highly monodisperse droplets through the breakup of hydrodynamically focused microthread in a microfluidic device," *Appl. Phys. Lett.* **85**, 3726 (2004).

³¹C. Charcosset, I. Limayem, and H. Fessi, "The membrane emulsification process—a review," *J. Chem. Technol. Biotechnol.* **79**, 209 (2004).

³²A. M. Gañán-Calvo, "Generation of steady liquid microthreads and micro-sized monodisperse sprays in gas streams," *Phys. Rev. Lett.* **80**, 285 (1998).

³³S. L. Anna, N. Bontoux, and H. A. Stone, "Formation of dispersions using 'flow focusing' in microchannels," *Appl. Phys. Lett.* **82**, 364 (2003).

³⁴T. Ward, M. Faivre, M. Abkarian, and H. A. Stone, "Microfluidic flow focusing: drop size and scaling in pressure versus flow rate-driven pumping," *Electrophoresis* **26**, 3716 (2005).

³⁵S. L. Anna and H. C. Mayer, "Microscale tipstreaming in a microfluidic flow focusing device," *Phys. Fluids* **18**, 121512 (2006).

³⁶A. S. Utada, A. Fernandez-Nieves, H. A. Stone, and D. A. Weitz, "Dripping to jetting transitions in coflowing liquid streams," *Phys. Rev. Lett.* **99**, 094502 (2007).

³⁷P. Guillot, A. Colin, A. S. Utada, and A. Ajdari, "Stability of a jet in confined pressure-driven biphasic flow at low Reynolds numbers," *Phys. Rev. Lett.* **99**, 104502 (2007).

³⁸T. G. Mason and J. Bibette, "Shear rupturing of droplets in complex fluids," *Langmuir* **13**, 4600 (1997).

³⁹K. Meleson, S. Graves, and T. G. Mason, "Formation of concentrated nanoemulsions by extreme shear," *Soft Mater.* **2**, 109–123 (2004).

⁴⁰T. G. Mason, J. N. Wilking, K. Meleson, C. B. Chang, and S. M. Graves, "Nanoemulsions: formation, structure, and physical properties," *J. Phys.: Condens. Matter* **18**, R635 (2006).

⁴¹J. N. Wilking and T. G. Mason, "Irreversible shear-induced vitrification of droplets into elastic nanoemulsions by extreme rupturing," *Phys. Rev. E* **75**, 041407 (2007).

⁴²J. D. Tice, A. D. Lyon, and R. F. Ismagilov, "Effect of viscosity on droplet formation and mixing in microfluidic channels," *Anal. Chim. Acta* **507**, 73 (2004).

⁴³B. Steinhaus, A. Q. Shen, and R. Sureskumar, "Dynamics of viscoelastic fluid filaments in microfluidic devices," *Phys. Fluids* **19**, 073103 (2007).

⁴⁴S. Shojaei-Zadeh and S. L. Anna, "Role of surface anchoring and geometric confinement on focal conic textures in smectic-A liquid crystals," *Langmuir* **22**, 9986 (2006).

⁴⁵L. E. Rodd, T. P. Scott, D. V. Boger, J. J. Cooper-white, and G. H. McKinley, "The inertio-elastic planar flow of low-viscosity elastic fluids in micro-fabricated geometries," *J. Non-Newtonian Fluid Mech.* **129**, 1 (2005).

⁴⁶A. Groisman, M. Enzelberger, and S. R. Quake, "Microfluidic memory and control devices," *Science* **300**, 955 (2003).

⁴⁷J. B. Knight, A. Vishwanath, J. P. Brody, and R. H. Austin, "Hydrodynamic focusing on a silicon chip: mixing nanoliters in microseconds," *Phys. Rev. Lett.* **80**, 3863 (1998).

⁴⁸H. H. Zuidema and G. W. Waters, "Ring method for the determination of interfacial tension," *Ind. Eng. Chem.* **13**, 312 (1941).

- ⁴⁹N. Rashidnia, R. Balasubramaniam, and D. Del Signore, "Interfacial tension measurement of immiscible liquids using a capillary tube," *AICHE J.* **38**, 615 (1992).
- ⁵⁰T. Cubaud and T. G. Mason, "A microfluidic aquarium," *Phys. Fluids* **19**, 091108 (2007).
- ⁵¹H. J. Subramani, H. K. Yeoh, R. Suryo, Q. Xu, B. Ambravaneswaran, and O. A. Basaran, "Simplicity and complexity in a dripping faucet," *Phys. Fluids* **18**, 032106 (2006).
- ⁵²B. Ambravaneswaran, H. J. Subramani, S. D. Philips, and O. A. Basaran, "Dripping-jetting transition in a dripping faucet," *Phys. Rev. Lett.* **93**, 034501 (2004).
- ⁵³H. A. Stone, "Dynamics of drop deformation and breakup in viscous fluids," *Annu. Rev. Fluid Mech.* **26**, 65 (1994).
- ⁵⁴D. D. Joseph and Y. Y. Renardy, *Fundamentals of Two-Fluid Dynamics. Part II: Lubricated Transport, Drops and Miscible Liquids* (Springer-Verlag, New York, 1993).
- ⁵⁵C. R. Carrigan and J. C. Eichelberger, "Zoning of magmas by viscosity in volcanic conduits," *Nature (London)* **343**, 248 (1990).
- ⁵⁶Q. Cao, A. L. Ventresca, K. R. Sreenivas, and A. K. Prasad, "Instability due to viscosity stratification downstream of a centerline injector," *Can. J. Chem. Eng.* **81**, 913 (2003).
- ⁵⁷F. M. White, *Viscous Fluid Flow* (McGraw-Hill, New York, 1991).
- ⁵⁸J. Eggers, "Nonlinear dynamics and breakup of free-surface flows," *Rev. Mod. Phys.* **69**, 865 (1997).
- ⁵⁹S. Tomotika, "On the instability of a cylindrical thread of a viscous liquid surrounded by another viscous fluid," *Proc. R. Soc. London, Ser. A* **150**, 322 (1935).
- ⁶⁰D. T. Papageorgiou, "On the breakup of viscous liquid threads," *Phys. Fluids* **7**, 1529 (1995).
- ⁶¹C. Pozrikidis, "Capillary instability and breakup of a viscous thread," *J. Eng. Math.* **36**, 255 (1999).
- ⁶²S. Senchenko and T. Bohr, "Shape and stability of a viscous thread," *Phys. Rev. E* **71**, 056301 (2005).
- ⁶³P. Huerre and P. A. Monkewitz, "Local and global instabilities in spatially developing flows," *Annu. Rev. Fluid Mech.* **22**, 473 (1990).
- ⁶⁴P. S. Hammond, "Nonlinear adjustment of a thin annular film of viscous fluid surrounding a thread of another within a circular pipe," *J. Fluid Mech.* **137**, 363 (1983).
- ⁶⁵J. G. Hagedorn, N. S. Martys, and J. F. Douglas, "Breakup of a fluid thread in a confined geometry: droplet-plug transition, perturbation sensitivity, and kinetic stabilization with confinement," *Phys. Rev. E* **69**, 056312 (2004).
- ⁶⁶D. Quéré, "Fluid coating on a fiber," *Annu. Rev. Fluid Mech.* **31**, 347 (1999).
- ⁶⁷J. Li and M. A. Fontelos, "Drop dynamics on the beads-on-string structure for viscoelastic jets: a numerical study," *Phys. Fluids* **15**, 922 (2003).
- ⁶⁸M. S. N. Oliveira, R. Yeh, and G. H. McKinley, "Iterated stretching, extensional rheology and formation of beads-on-a-string structures in polymer solutions," *J. Non-Newtonian Fluid Mech.* **137**, 137 (2006).
- ⁶⁹P. Garstecki, H. A. Stone, and G. W. Whitesides, "Mechanism for flow-rate controlled breakup in confined geometries: a route to monodisperse emulsions," *Phys. Rev. Lett.* **94**, 164501 (2005).
- ⁷⁰T. A. Kowalewski, "On the separation of droplets from a liquid jet," *Fluid Dyn. Res.* **17**, 121 (1995).
- ⁷¹D. Henderson, H. Segur, L. B. Smolka, and M. Wadati, "The motion of a falling liquid filament," *Phys. Fluids* **12**, 550 (2000).
- ⁷²J. R. Lister and H. A. Stone, "Capillary breakup of a viscous thread surrounded by another viscous fluid," *Phys. Fluids* **10**, 2758 (1998).
- ⁷³I. Cohen, M. P. Brenner, J. Eggers, and S. R. Nagel, "Two fluid drop snap-off problem: experiment and theory," *Phys. Rev. Lett.* **83**, 1147 (1999).
- ⁷⁴J. H. Snoeijer, G. Delon, M. Fermigier, and B. Andreotti, "Avoided critical behavior in dynamically forced wetting," *Phys. Rev. Lett.* **96**, 174504 (2006).
- ⁷⁵N. Le Grand, A. Daerr, and L. Limat, "Shape and motion of drops sliding down in inclined plane," *J. Fluid Mech.* **541**, 293 (2005).
- ⁷⁶P. G. de Gennes, "Wetting—statics and dynamics," *Rev. Mod. Phys.* **57**, 827 (1985).
- ⁷⁷T. Cubaud, U. Ulmanella, and C.-M. Ho, "Two-phase flow in microchannels with surface modifications," *Fluid Dyn. Res.* **38**, 772 (2006).